A Simplified Linear Framework for Interpreting Patterns of Northern Hemisphere Wintertime Climate Variability

ROBERTA QUADRELLI AND JOHN M. WALLACE

University of Washington, Seattle, Washington

(Manuscript received 19 May 2003, in final form 7 April 2004)

ABSTRACT

The principal patterns of variability of the extratropical Northern Hemisphere (NH) wintertime circulation are examined, based on 42 yr of data from the NCAR–NCEP reanalyses. The two-dimensional phase space defined by the two leading PCs of the monthly mean sea level pressure (SLP) field poleward of 20°N is used as a basis for surveying the structure of the geopotential height and surface air temperature (SAT) fields. Together these two patterns account for roughly half the variance of SLP on interannual time scales and longer, and virtually all the planetary-scale SLP trends over the 42-yr period of record. The leading EOF corresponds to the NH annular mode (NAM), and the second EOF resembles the Pacific–North America (PNA) pattern.

The leading EOF of the monthly mean geopotential height field at various levels throughout the troposphere and lower stratosphere is well represented by linear combinations of these two SLP patterns, as are the intraseasonal and interannual SLP fields, the NAM, the North Atlantic Oscillation (NAO), the PNA pattern, the pattern corresponding to the North Pacific index (NP), the cold ocean–warm land (COWL) pattern, the seasaw between the depths of the Aleutian and Icelandic lows (AIS), and the leading EOFs of lower-tropospheric temperature and midtropospheric wind. The combined influence of these patterns on temperature and rainfall and other variables can be represented in terms of compact vectorial plots.

Interesting differences emerge when the EOF analysis is performed separately on the intraseasonal and interannual components of the NH SLP field. The former patterns appear to be hemispherically trapped, whereas the latter appear to be reflections of global structures, with ENSO clearly dominating the structure of interannual EOF2.

1. Introduction

The climate dynamics literature abounds with patterns of variability; some labeled as teleconnection patterns, oscillations, clusters, seesaws, or modes; many others known only by mode number. The documentation of structures in sea level pressure (SLP) and upper-tropospheric geopotential height fields has proceeded largely independently, each yielding its own set of patterns.

The different analysis techniques used in climate dynamics research also yield different patterns, and even the same technique can yield quite different results, depending upon whether it is applied to a total field or to the zonally symmetric or asymmetric components of that field. The patterns that have emerged in various studies have also been conditioned by the spatial domain of the analysis, the manner in which seasonality is treated, and the time interval over which the data are averaged before the analysis is performed.

Appendix B in Barnston and Livezey (1987) lists some of the patterns of variability identified prior to that time. Subsequent entries include the patterns associated with Trenberth and Hurrell's (1994) North Pacific index, Mantua et al.'s (1997) Pacific decadal oscillation (PDO), Thompson and Wallace's (1998, 2000) Arctic Oscillation (AO) or Northern Hemisphere annular mode (NAM), Honda and Nakamura's (2001) Aleutian–Icelandic seesaw (AIS), and Wallace et al.'s (1995) ''cold ocean–warm land'' (COWL) pattern. In some cases, the same term has been used as a label for two or more patterns.[1]

It would simplify the climate dynamics literature if this plethora of patterns could somehow be distilled or at least placed in a common framework that would allow for systematic intercomparison of the spatial patterns and their associated time series. In this study we will show that many of the Northern Hemisphere (NH) extratropical wintertime patterns that have been identified on the basis of monthly mean SLP and geopotential height data project strongly upon the two-dimensional

Corresponding author address: Roberta Quadrelli, JISAO, Dept. of Atmospheric Sciences, University of Washington, Box 354235, Seattle, WA 98195-4235.
E-mail: roberta@atmos.washington.edu

[1] For example, compare the patterns referred to as the AO by Thompson and Wallace (1998), Wang and Ikeda (2000), and Rogers and McHugh (2002).

phase space defined by the leading empirical orthogonal functions (EOFs)[2] of the monthly mean SLP field, here defined on the basis of winter (December through March) monthly data, 1958–99. In a similar manner, the time-varying indices of these patterns project strongly onto the leading principal components (PCs) of the SLP field. We will also show that the leading EOFs and PCs of the geopotential height field at levels throughout the troposphere project strongly onto the phase space defined by the EOFs and PCs of the SLP field, and that the same is true for SLP EOFs and PCs derived from seasonal-mean data, and for the spatial pattern of SLP trends over the Northern Hemisphere.

The paper is organized as follows. Data sources and analysis techniques are described in the next section. Section 3 describes the spatial and temporal ''phase space'' defined by the two leading EOFs of the wintertime monthly mean sea level pressure field and their associated principal component time series. Sections 4 and 5 document the linear relationship between a number of previously identified patterns in terms of their projections in space and time upon these two-dimensional phase spaces. Section 6 compares the SLP EOFs with the EOFs of the geopotential height field at various levels. Section 7 discusses the frequency dependence of these two-dimensional phase space representations, and section 8 shows that trends in wintertime SLP and land surface air temperature over the last few decades project strongly onto the two-dimensional EOF phase space. Results are discussed in section 9 and concluding remarks are given in the final section.

2. Data and analysis techniques

The primary dataset used in this study is the National Centers for Environmental Prediction–National Center for Atmospheric Research (NCEP–NCAR) reanalysis (Kalnay et al. 1996) obtained from the National Oceanic and Atmospheric Administration (NOAA) Climate Diagnostic Center (CDC). The data are gridded on a 2.5° latitude × 2.5° longitude mesh. The fields used are sea level pressure, 850-, 500-, 250-, 200-, 100-, 50-, 30-, and 10-hPa geopotential height, 500-hPa wind, and 850-hPa temperature for the 42-yr period of record 1958–99. An additional SLP dataset for the extended period 1925–99 (Trenberth and Paolino 1980) is used to test the robustness of results relating to interannual and longer-term variability. We also make use of land temperature and precipitation datasets produced at the University of Delaware by Willmott and collaborators, available from http://climate.geog.udel.edu/~climate/html_pages/archive.html for the period 1950–99: the newest version with ''climatologically aided interpolation'' (Willmott and Robeson 1995); monthly values from 1958 through 1999.

The analysis is restricted to the winter season, defined as extending from December through March (DJFM), a total of 168 months. Principal component analysis (PCA) is performed on the covariance matrix of monthly DJFM SLP anomalies. The anomalies are area-weighted by the square root of the cosine of latitude, and only the region north of 20°N is included in the analysis. The corresponding spatial patterns that we will refer to as EOFs are derived by linearly regressing the monthly SLP field upon these principal component time series. The leading two principal component (PC1 and PC2) time series and the associated EOFs may be viewed as comprising the two-dimensional temporal and spatial phase spaces upon which various time series and spatial patterns can be projected, as described in more detail in the next section.

We are aware of the existence of spurious discontinuities in the NCEP–NCAR reanalyses associated with the introduction of satellite data during the 1970s, but the contribution of these features to the month-to-month variance of the wintertime data is very small. We have verified that the leading EOF of the geopotential height field at the 1000-, 500-, and 50-hPa levels is relatively insensitive to these discontinuities by computing it separately for the periods 1958–78 and 1979–99. In all cases the patterns were found to be highly consistent.

Time-varying indices are used to represent a number of previously identified patterns of climate variability. Following Hurrell (1995), the North Atlantic Oscillation (NAO) is defined as seasonal (December through March) means of the difference between the standardized SLP at Stykkisholmur, Iceland, and Lisbon, Portugal (available online at: http://www.cgd.ucar.edu/~jhurrell/nao.stat.html).

Monthly values of the index are obtained by forming time series of SLP for the NCEP grid points located closest to the Iceland and Lisbon centers of action of the NAO. The index of the Pacific–North America (PNA) pattern is computed from the 500-hPa winter monthly anomalies at specified grid points following the definition given in Wallace and Gutzler (1981, hereafter WG). The depths of the Aleutian and Icelandic lows are defined as SLP anomalies (with sign reversed) averaged over areas surrounding their respective centers of action in the climatological mean SLP field in which the temporal correlation with the center exceeds 0.8. The North Pacific index (Trenberth and Hurrell 1994) is obtained by removing the climatological-mean month-to-month variability from the index available online at http://www.cgd.ucar.edu/~jhurrell/np.html.

Following Wallace et al. (1995) the cold ocean–warm land pattern index is defined as the NH mean surface air temperature poleward of 20°N using the University of Delaware dataset, based on land data only. The Southern Oscillation index (SOI) is the difference between standardized SLP time series at Tahiti and Darwin, as defined

[2] The PC time series and the associated spatial patterns called EOFs have been widely used as basis for identifying the dominant patterns of climate variability. Examples include the studies of Kutzbach (1970), Kidson (1975), and Trenberth and Paolino (1981).

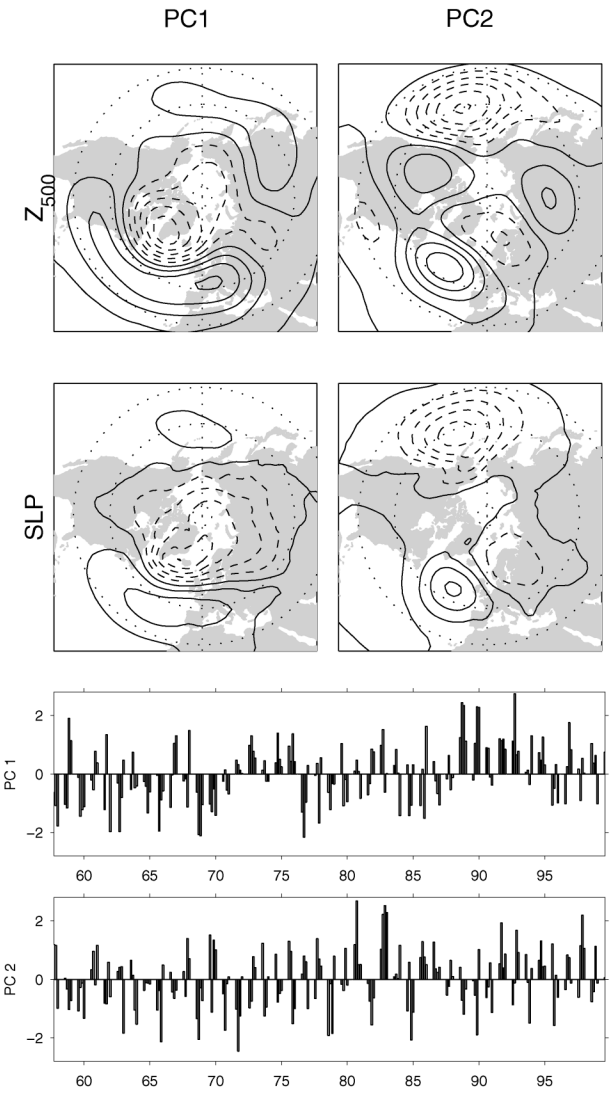

FIG. 1. Monthly mean 500-hPa height and SLP fields regressed on standardized PCs 1 and 2 of monthly mean DJFM SLP anomalies poleward of 20°N, based on data for 1958–99. Contour interval 1.5 hPa for SLP and 15 m for 500-hPa height; negative contours are dashed. Here and in all the subsequent maps the latitude circle plotted corresponds to 30° and 45°N. (bottom) Time series of the standardized PCs 1 and 2, DJFM values only.

in Trenberth (1984). Monthly data of the SOI index calculated by NCEP, and based on the University of East Anglia data, may be obtained online from http://tao.atmos.washington.edu/pacs/additional_analyses/soi.html.

The index of the leading PC of the monthly vertically and zonally averaged zonal wind in the domain extending from 10° to 80°N for the winters 1976–99 (December through March), computed after linearly removing the ENSO variability, as represented by a multivariate index, is the same as in Lorenz and Hartmann (2003).

3. The SLP EOF1−EOF2 phase space

Figure 1 shows monthly 500-hPa height (top) and SLP fields (bottom) regressed upon PCs 1 and 2 of monthly mean DJFM SLP anomalies poleward of 20°N. Explaining 24% and 13% of the total variance of the field, respectively, these EOFs are well separated from one another by the criterion of North et al. (1982) and the second EOF is well separated from the third, which accounts for only 9% of the variance.

Based on the definition of Thompson and Wallace (1998), the first pattern corresponds to the Arctic Oscillation, referred to in subsequent papers as the Northern Hemisphere annular mode. The pattern formed by regressing the 500-hPa-height field onto the second PC bears a strong resemblance to the Pacific–North America pattern, defined in WG, and its associated PC time series is strongly correlated with the PNA index ($r = 0.79$). However, the 500-hPa pattern derived from the SLP PC is characterized by more prominent features over the North Atlantic and Eurasia than the pattern described by WG. The one-point regression map for its Pacific center of action (45°N, 165°W) exhibits weak centers of action in those same regions (e.g., see Fig. 4 of Wallace and Thompson 2002). To distinguish SLP EOF2 from WG's PNA pattern we will refer to it as the *PNA-like* pattern. The polarity of EOF1/PC1 is chosen to be consistent with the usual sign convention of the NAM and the polarity of the PNA-like second EOF is consistent with that of WG's PNA pattern.

Table 1 shows the ratio of the interannual to the intraseasonal variances of monthly mean DJFM data, and the 1-month-lag autocorrelation, for each of the first 10 monthly DJFM NH SLP PCs. By both measures, the two leading patterns are substantially redder (i.e., exhibit a larger fraction of temporal variance in lower frequencies of the spectrum) than subsequent patterns and are therefore of particular interest from the viewpoint of climate. It is interesting to note that the next reddest mode (the sixth, not shown) exhibits a vertical structure reminiscent of the NAM, but the node is located farther north and, as for the NAM, the associated zonally averaged zonal wind perturbations amplify with height into the stratosphere.

TABLE 1. Ratio of the interannual to the intraseasonal variances (row 1) and 1-month-lag autocorrelation of monthly DJFM SLP PCs 1–10 (row 2).

	PC1	PC2	PC3	PC4	PC5	PC6	PC7	PC8	PC9	PC10
Variance ratio	1.01	0.77	0.33	0.46	0.37	0.63	0.39	0.45	0.40	0.39
Autocorrelation	0.45	0.31	0.07	0.21	0.10	0.22	0.09	0.15	0.06	0.06

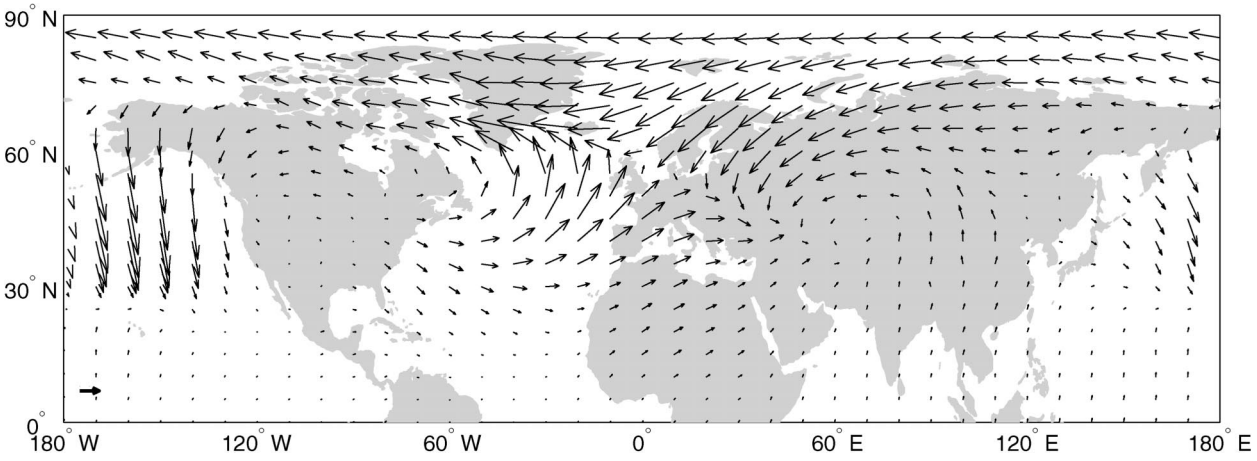

FIG. 2. Vectorial representation of regression coefficients of monthly mean SLP upon PCs 1 (*x* component) and 2 (*y* component) of monthly DJFM SLP anomalies. The vector in the lower-left corner corresponds to 3 hPa per unit std dev of the PC time series.

Figure 2 shows the SLP field regressed onto standardized SLP PCs 1 and 2, in a vectorial format. The lengths of vectors are proportional to the combined root-mean-square amplitude of the SLP fluctuations attributable to the two modes. The NAM is dominant over the Arctic and over the subtropical Atlantic and Mediterranean while the PNA-like pattern is dominant over the Pacific sector.

The orientation of the *x* and *y* axes in this two-dimensional phase space defined by the leading EOFs or PCs is subject to some degree of uncertainty due to the sampling variability inherent in a 42-yr record. To characterize that uncertainty, we generated 1000 synthetic datasets and projected the leading EOF derived from each of them onto the two-dimensional phase space defined by EOFs 1 and 2 of the observations. Results are shown in Fig. 3.[3] Based on the analysis of North et al. (1982) and the empirical results of Cheng et al. (1995) it is expected that most of the sample-to-sample variability in the structure of EOF1 will be due to mixing between EOFs 1 and 2. If this is, in fact, the case, then the points for the individual samples should tend to lie just inside the unit circle in Fig. 3 and, in fact, they do. The dispersion of the points about the *x* axis in this two-dimensional phase space is a measure of the sampling error in EOF1.

Based on these results, the standard error in the determination of the angle of EOF1 in this two-dimensional phase space is estimated to be 7°. Hence, EOFs separated by more than 14° (two standard deviations) in this two-dimensional phase space may be regarded as significantly different at the 95% confidence level.

4. Projections of spatial patterns

Figure 4 shows the area-weighted spatial correlations between EOFs 1 and 2 and the spatial patterns of SLP anomalies associated with selected patterns of variability, as indicated, within the domain poleward of 20°N. Vectors that extend all the way out to the unit circle are indicative of spatial patterns that can be perfectly represented as ''best fit'' linear combinations of EOFs 1 and 2 and hence lie within the same plane in multidimensional phase space as they do. The vectors for the NAO and the PNA pattern extend nearly all the way out to the unit circle: they are correlated with the respective best-fit linear correlations of EOFs 1 and 2 at levels 0.99 and 0.93, respectively. These strong correlations, together with the near orthogonality of the NAO and PNA vectors is consistent with the interpretation in Ambaum et al. (2001) and Wallace and Thompson (2002) in which the NAO/PNA and the NAM/PNA-like pattern paradigms are viewed as alternative representations of the dominant modes of variability of the Northern Hemisphere wintertime circulation. The two pairs of coordinate axes differ by 15°–22°, depending on whether the NAO or PNA is used to define the NAO/PNA coordinate system. The separation between the EOF1/EOF2 axes and the NAO/PNA axes is significant in terms of the criterion discussed at the end of the previous section.

The configurations of the vectors in Fig. 4 resemble the schematic in Fig. 3 of Wallace and Thompson (2002), but rotated clockwise so that EOF1 rather than the NAO coincides with the *x* axis. The 15° counterclockwise rotation of the NAO relative to the *x* axis is just sufficient to eliminate the weak Pacific center of action in EOF1, leaving a sectoral North Atlantic pattern. In a similar manner, the counterclockwise rotation

[3] The synthetic datasets were generated as follows: For each of the 168 observed PC time series, a random normal, first-order autoregressive time series was generated, whose lag-1 month-to-month autocorrelation within a given winter matches that of the observed PC. (No attempt was made to match the observed winter-to-winter autocorrelation.) EOF analysis was performed upon the synthetic dataset consisting of 168 randomly varying PCs, and the leading EOF was projected (using area-weighted spatial correlation coefficients) onto the phase space defined by EOFs 1 and 2 of the observations.

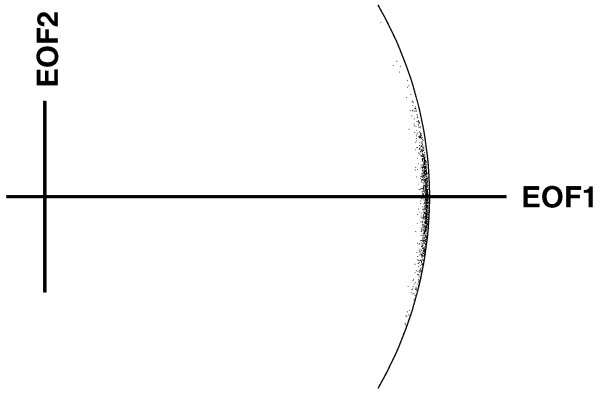

FIG. 3. Phase space defined by EOFs 1 and 2 of monthly DJFM SLP anomalies for the period 1958–99. The cloud of dots represents projections of the leading EOFs of 168-month datasets derived from Monte Carlo experiments, as defined by their correlation coefficients. The dots lie just inside the circle of unit radius.

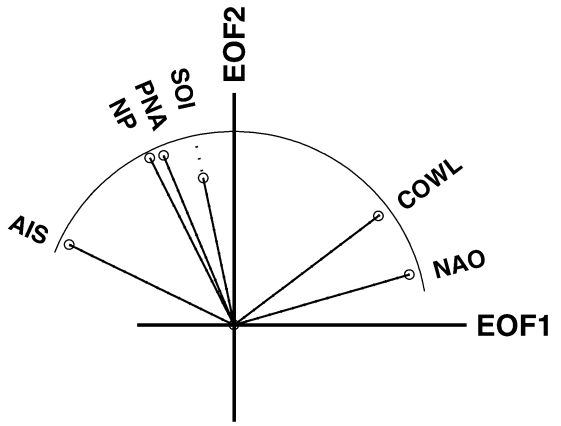

FIG. 4. Projections (area-weighted spatial correlations) of patterns associated with various indices on the phase space defined by the two leading EOFs of monthly DJFM NH SLP anomalies, north of 20°N. For reference, a circle of unit radius is shown in the plots. Positive values of the EOFs denote polarities indicated in Fig. 1.

of the PNA pattern relative to the *y* axis weakens the Atlantic/Eurasian wave train in EOF2, but in this case the cancellation is incomplete (i.e., the PNA pattern as defined in WG lies slightly outside this two-dimensional phase space). The SLP regression pattern for Trenberth and Hurrell's (1994) North Pacific (NP) SLP index, the area-weighted sea level pressure over the region 30°–65°N, 160°E–140°W, which corresponds to the region covered by the climatological mean Aleutian low, lies closer to the phase space: it is correlated with the best-fit linear combination of EOFs1 and 2 at a level of 0.97 compared to 0.94 for the pattern derived from WG's PNA index. The spatial patterns of both SLP and 500-hPa height defined by WG's PNA index and Trenberth and Hurrell's NP SLP index are correlated with one another at a level of 0.97. Hence, it is clear that the two indices are representing the time variability of the same three-dimensional pattern.

Vectors that lie within the first quadrant in Fig. 4 denote polarities of EOFs 1 and 2 in the same sense as in Fig. 1, commonly referred to as the ''high index'' polarity. Angles between the NAO and PNA vectors are indicative of anomalously strong Icelandic and Aleutian lows. Angles in the quadrants extending counterclockwise from the PNA and clockwise from the NAO are indicative of a negative correlation or ''seesaw'' between the depth of the Icelandic and Aleutian lows. The Aleutian–Icelandic seesaw investigated by Honda and Nakamura (2001) and Honda et al. (2001) lies nearly entirely within this phase space, at angles (150°, −30°).

The SLP signature of the Southern Oscillation, obtained by regressing SLP poleward of 20°N upon the time series of the Southern Oscillation index, does not project as strongly upon EOFs 1 and 2 of the monthly data as the other patterns considered in this section do.

The ''cold land–warm ocean (COWL) pattern,'' defined by regressing SLP onto the monthly time series of hemispheric mean land temperature (Wallace et al. 1995), is correlated with the best-fit linear combination of EOFs 1 and 2 at a level of 0.93. The orientation of the COWL pattern, near the middle of the first quadrant in Fig. 4, is consistent with the observed tendency for the Icelandic and Aleutian lows to be deeper than normal during those months in which hemispheric mean temperature is abnormally warm. These relationships are clearly evident in maps of surface air temperature (SAT) and SLP regressed upon hemispheric mean land SAT, shown in Fig. 5.

5. Projections of time series

In analogy with Fourier analysis, the temporal variability of a prescribed spatial pattern $P(x)$ may be described in terms of a ''projection index'' $I(t)$ formed by projecting the observed field $Z(x, t)$ onto the pattern, that is,

$$I(t) = \iint P(x)Z(x, t)\, dA, \qquad (1)$$

where A is area and the domain of integration is the Northern Hemisphere poleward of 20°N. For convenience, projection indices are standardized.

Figure 6a shows the temporal correlations between the projection indices and PCs1 and 2 of the SLP field in a vectorial format. The angles and lengths of the vectors are comparable to those for the spatial correlations shown in the previous figure. That the correlations are very close to 1 implies that the time variability of these patterns can be well represented by linear combinations of PCs1 and 2 of NH SLP.

Many of the patterns in the climate dynamics literature are defined on the basis of ''primitive indices''; that is, time series based on prescribed formulas. For example, the NAO, the PNA pattern, and the Southern Oscillation are defined on the basis of station or grid-point data at specified locations; the NP and AIS are

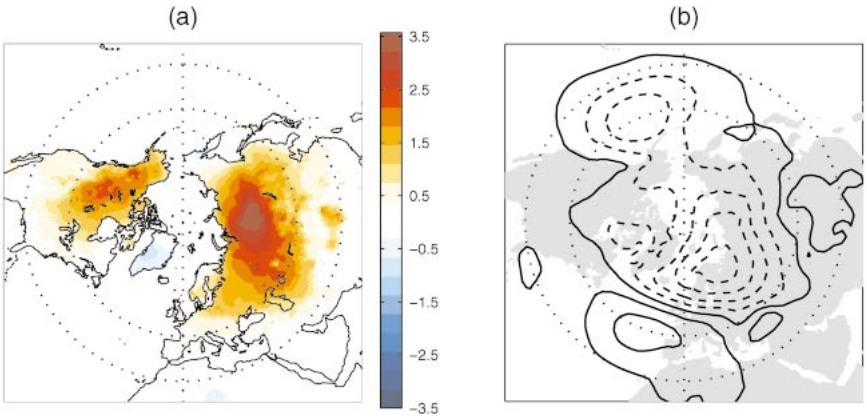

FIG. 5. (a) Surface air temperature and (b) sea level pressure regressed upon an index of hemispheric mean land surface air temperature. SLP contour interval 1 hPa; negative contours are dashed.

based on SLP averaged over specified regions; the COWL SLP pattern is formed by projecting the SLP field onto the time series of hemispheric mean land temperature. The index comes first (hence the term primitive) and the associated spatial pattern is derived from it by compositing or by performing linear regression. Projection indices and primitive indices are one and the same only for the special case of EOFs and PCs.

Since the focus of this paper is on spatial patterns, projection indices are the natural measure of the temporal variability of the patterns. Nevertheless, primitive indices are of interest because relatively long time series of data are available only at specific locations, corresponding to observing stations or proxy records. The correlation coefficients between an expanded set of primitive indices and the leading PCs of the SLP field are shown in Fig. 6b. The angles for the primitive indices are very similar to those for the respective projection indices, but the correlations with PCs1 and 2 are generally weaker, either because the primitive indices are based on highly simplified representations of the patterns (as in the case of the NAO, PNA, and AIS), or because they are only indirectly related to the NH SLP field (as in the case of the COWL pattern).

The relationship between the PNA pattern defined by WG and the NP index defined in Trenberth and Hurrell (1994) provides an example of the subtle, but sometimes important distinctions between projection indices and primitive indices. Both patterns are defined on the basis of their primitive indices, which are correlated with one another at a level of 0.86. The corresponding projection indices based on their SLP patterns are correlated with one another at a level of 0.99. Hence the primitive indices do not fully reflect the almost complete redundancy between the patterns whose variability they are designed to represent.

To investigate whether the primitive indices contain any information concerning spatial patterns of SLP variability that is linearly independent of the leading EOFs, we formed residual time series, from which the variability associated with PCs 1 and 2 was removed by a least squares best fit. Results for the NAO and PNA indices are shown in Fig. 7. The negative center of action over Scandinavia in the pattern for the NAO re-

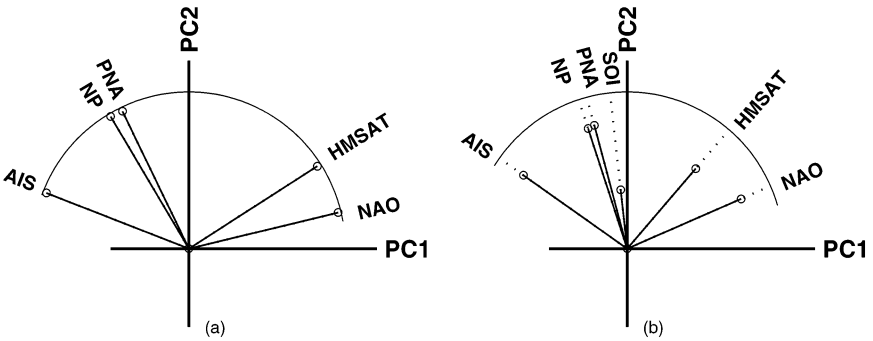

FIG. 6. Projections of various indices on the phase space defined by the two leading PCs of monthly DJFM NH SLP anomalies. (a) Temporal correlations of projection indices and (b) temporal correlations of primitive indices with the SLP PCs. Positive values of the PCs denote polarities indicated in Fig. 1.

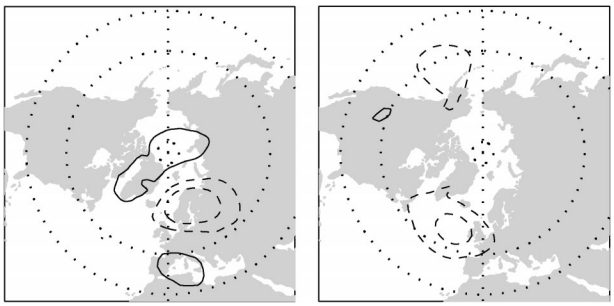

FIG. 7. Monthly mean SLP fields regressed on residual time series formed by subtracting from the primitive indices of (left) NAO and (right) PNA the variability associated with PCs 1 and 2. Contour interval 1.5 hPa; negative contours are dashed.

sidual index indicates that the isobars in the pattern based on the primitive index curve more cyclonically over that region than the isobars in the NAO as represented in the 2D phase space. The negative center over the North Atlantic in the pattern based on the WG PNA residual index reflects the failure of the WG PNA index to capture the negative correlations between geopotential height in the Pacific and Atlantic sectors. With the exception of these regional features, regression maps based on the primitive indices and the best-fit linear combinations of PCs 1 and 2 are virtually identical.

Whenever reliable gridded data are available for constructing them, the projection indices which incorporate information from the complete gridded fields offer a more faithful representation of the time variability of the patterns.

6. Projections of EOFs of the geopotential height field onto the 2D phase space

The leading EOFs and PCs of geopotential height on various pressure levels also bear a close relationship to the two leading SLP patterns. Figure 8 shows correlations between the two leading EOFs and PCs of the 500- and 50-hPa height field and their SLP counterparts. The 500-hPa height PCs are strongly correlated with the SLP PCs, but when projected onto the phase space of SLP PCs they are rotated clockwise by an angle of ~25°. The pattern obtained by regressing SLP onto the leading PC of 50-hPa height is virtually identical to the leading EOF of SLP, but the temporal correlation coefficient between the corresponding PCs is, of course, much weaker.

The subtle changes in the PCs of the geopotential height field from level to level are documented in more detail in Fig. 9. Figure 9a shows the clockwise rotation of the leading PC of middle- and upper-tropospheric geopotential height relative to PC1 of SLP. Figure 9b shows the relative prominence of the leading EOFs at each level. The fraction of the variance explained by the leading PC is generally higher in the stratosphere than in the troposphere, and it exhibits a distinct minimum in the middle to upper troposphere. It is evident from the figure that the level-to-level differences in the fraction of variance explained by EOF1 are not a reflection of a trade-off of variance among the leading EOFs. Rather, they are suggestive of a greater complexity of the anomalies in the middle- and upper-tropospheric geopotential height field compared to those in the SLP and stratospheric geopotential height fields; that is, the larger number of spatial degrees of freedom.

Consistent with the smaller fraction of the variance explained by the leading EOF of the 500-hPa height field compared to that of the SLP field, the rms error in the angle of the *x* axis in the two-dimensional phase space was found to be larger in the Monte Carlo test described in section 3 (17° versus 7°). This result is consistent with the large sampling variability of the 500-hPa height EOFs reported by Cheng and Wallace (1993) (their Fig. 2).

Figure 9c shows the fraction of the geopotential height variance at each level that is explained by PCs 1 and 2 of SLP. In combination, the two SLP PCs explain ~30% of the geopotential height variance at levels all the way up to 100 hPa. Note the secondary maximum

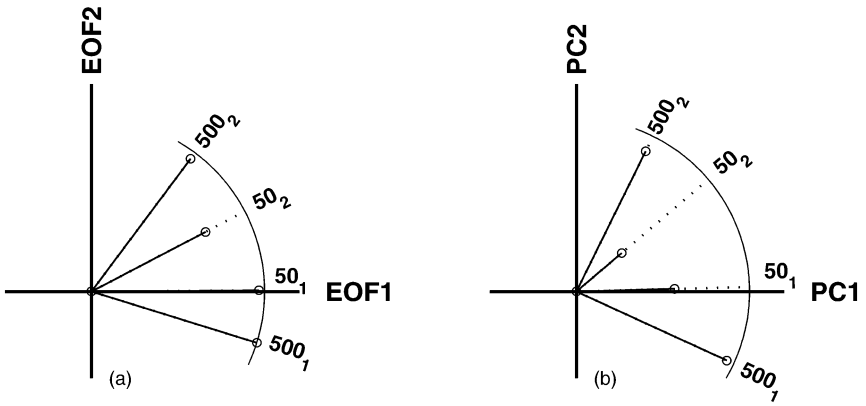

FIG. 8. As in Figs. 4 and 6 but for the leading EOFs/PCs of 50- and 500-hPa height, as indicated.

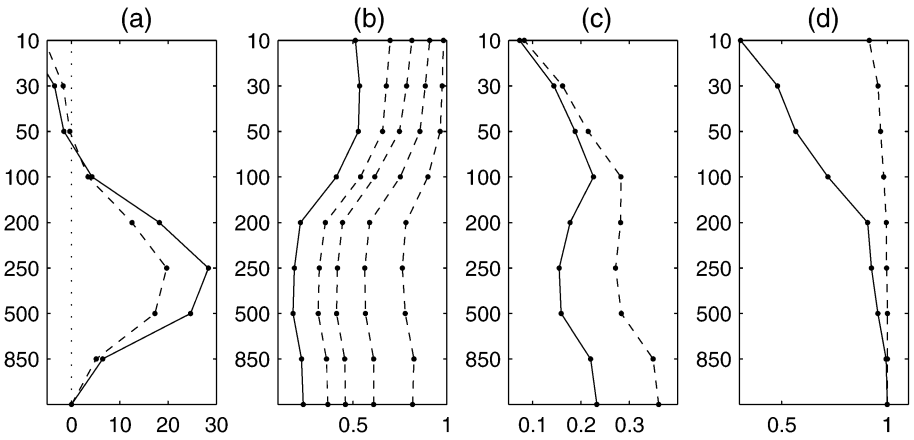

FIG. 9. Leading EOFs of the geopotential height field at 10 vertical levels. (a) Clockwise angle (degrees) from the *x* axis of the phase space of Fig. 4 defined by the leading mode at each level (temporal phase space solid; spatial phase space dashed). (b) Fraction of the variance explained by the first, the first 2, the first 3, the first 5, and the first 10 EOFs at each level. (c) Fraction of the variance of monthly mean of geopotential height at each level explained SLP PC1 (solid), SLP PC1 + PC2 (dashed). (d) Correlation between the best-fit linear combination of the two leading SLP EOF/PCs and the first EOF/PC at each level [temporal (solid); spatial (dashed)].

in the fraction of the variance explained by SLP PC1 at the 100-hPa level.

Figure 9d shows spatial and temporal correlation coefficients between the leading EOF/PC of the geopotential height field at each level and the least squares best fit of the two leading EOF/PCs of the SLP fields. The spatial correlations are nearly perfect at all levels. The temporal correlations with PC1 of SLP decrease monotonically with height, remaining quite strong throughout the depth of the troposphere, and declining more rapidly with height in the lower stratosphere.

In Molteni et al. (1988) the leading EOFs of the eddy component of the 500-hPa height field are used as basis functions. In contrast to the leading EOF of the total 500-hPa height field, the leading EOF of the eddy field shown in Fig. 10 lies in the second quadrant, in virtually the same direction as the PNA pattern in Fig. 4. The PC time series of this pattern is well correlated with WG's index of the PNA pattern ($r = 0.81$). Not surprisingly, the leading PC of the zonally symmetric component of the 500-hPa height field lies close to the *x* axis (i.e., the NAM), as does the leading PC of vertically and zonally averaged zonal wind as defined in Lorenz and Hartmann (2003). It is evident that the PCs of the zonal mean and eddy components tend to be negatively correlated to some degree.

7. Frequency dependence of the 2D phase space

This section deals with four different aspects of the frequency dependence of the two leading EOFs of the SLP field:

- their combined contribution to the total hemispherically integrated variance,

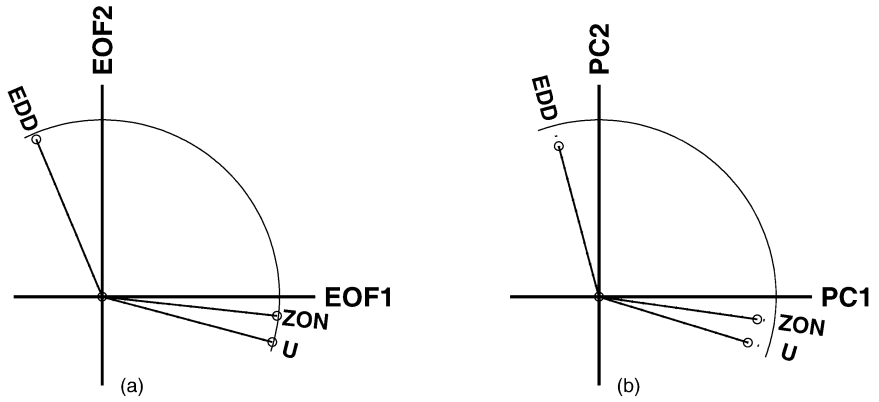

FIG. 10. As in Fig. 4 but for the leading EOF of the zonal and eddy component of the 500-hPa field, and for the leading PC of vertically and zonally averaged zonal wind (*U*) as defined in Lorenz and Hartmann (2003).

- the orientation of the two-dimensional phase space that they define,
- their orientation within that phase space, and
- their relation to the global SLP field.

Table 2 shows the hemispherically integrated variance of the monthly, seasonal, and 5-yr mean wintertime (DJFM) variability of the SLP field, and the fraction of that variance explained by the two leading PCs. In the second column the monthly mean SLP PCs are averaged, and in the third column new PCs are defined on the basis of data averaged, as indicated, for each row. In both columns the fraction of explained variance increases with averaging interval. That the percentages in the two columns are similar implies that the two-dimensional phase spaces defined by the monthly, seasonal, and 5-yr mean EOF's must also be quite similar.

Another way of documenting the increasing prominence of the NAM and the PNA-like pattern with increasing time scale of the fluctuations is through a comparison of the spatial patterns of temporal variance. The combined variance of EOFs 1 and 2 of monthly mean SLP is shown in Fig. 11, together with the total variance of the monthly, seasonal, and 5-yr mean SLP field. The

TABLE 2. SLP variance north of 20°N of monthly, seasonal, and 5-yr averaged data: ratio between area-weighted variance of averaged data and original monthly variance (first column); percentage of the variance explained by the combined leading two SLP PCs: averaged monthly PCs (second column), and PCs of averaged data (third column).

	v/v_m	$(\text{PC1} + \text{PC2})_m$	PC1 + PC2
Monthly	1	36	36
Seasonal	0.39	49	51
5-yr mean	0.15	72	74

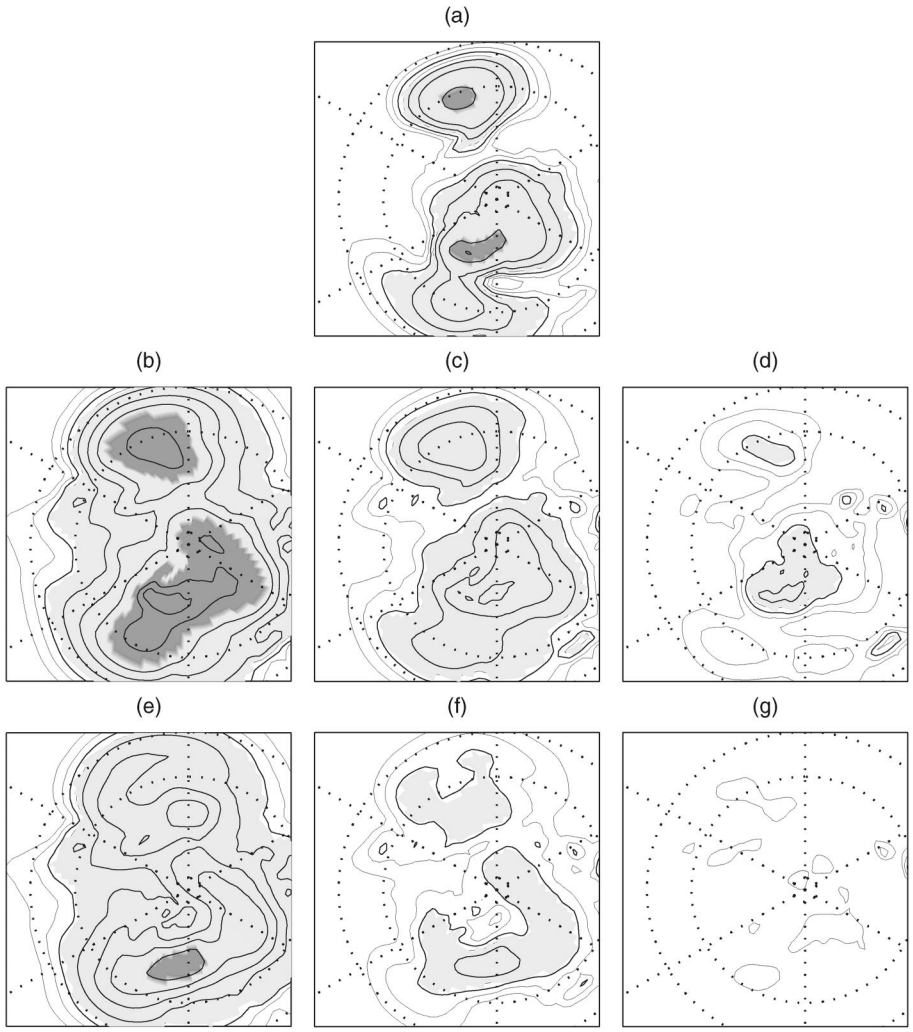

FIG. 11. Variance maps of SLP data: (a) monthly variance explained by combined monthly PCs 1 and 2; total variance of observed (b) monthly, (c) seasonal mean, (d) 5-yr mean data. (e), (f), (g) Residual variances in (b), (c), (d) after removing the contribution of PCs 1 and 2. Contours are at 6, 12, 20, 30, 42, 56, 72 hPa^2; the 6 and 42 hPa^2 contours are bold; additional light contours are at 2, 4, 9 hPa^2.

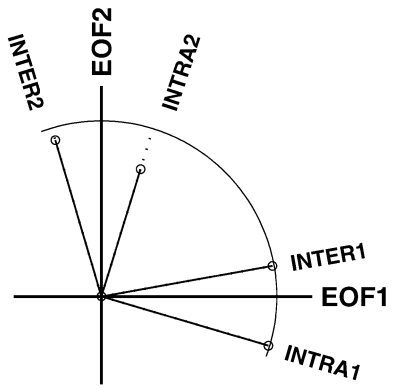

FIG. 12. As in Fig. 4a but for EOFs of intraseasonal and interannual SLP fluctuations for the NH north of 20°N.

shape of the leading EOFs of monthly mean SLP is evident in all three total variance maps, and it is particularly prominent in those representative of the lower-frequency variability. The corresponding residual fields, shown in the bottom row of Fig. 11, were formed by regressing out the pattern in Fig. 11a from the three total variance patterns. They lack the focused ''center of action'' that characterize the variance maps in which all EOFs are included.

EOF analysis was performed on the seasonal (DJFM) mean and intraseasonal (departures of monthly DJFM means from their respective winter season means) SLP fields. Figure 12 shows the projections of the leading intraseasonal and interannual EOFs onto the plane of the monthly EOFs.

The interannual and intraseasonal EOF1s are seen to be linear combinations of the corresponding monthly EOFs, rotated counterclockwise by 16° and clockwise by 10°, respectively, relative to the leading EOF of monthly mean SLP, as shown in Fig. 12. Hence, they differ from one another by 26°. In only 6% of a set of the Monte Carlo simulations, designed as described in section 2, was the angular separation as large as the observed. Hence, the differences appear to be real.

The patterns of EOF1 for the interannual versus the

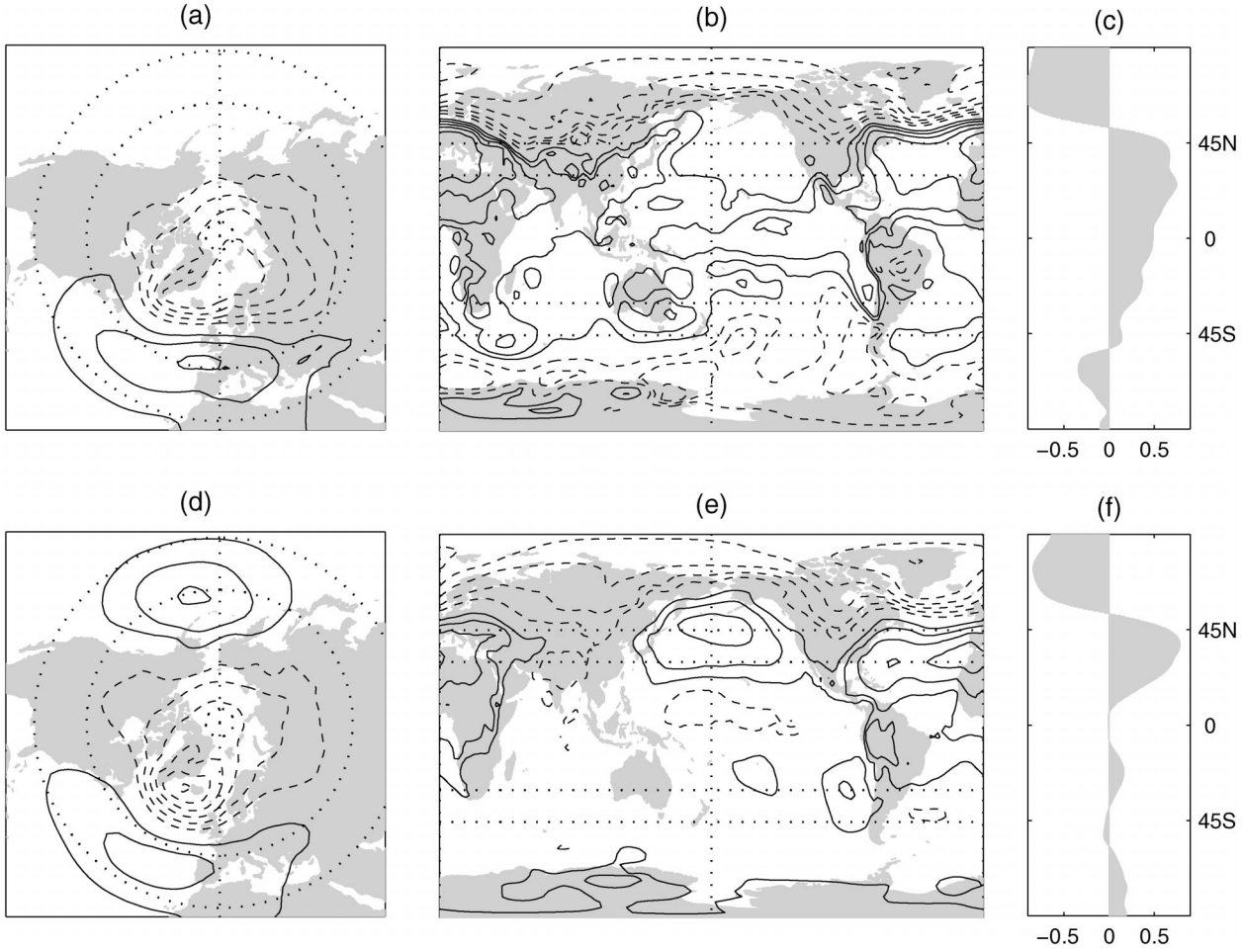

FIG. 13. The leading EOF of (a) winter-averaged and (d) intraseasonal NH SLP. (a), (d) Hemispheric regression maps; (b), (e) the corresponding global correlation maps for SLP; (c), (f) meridional profile of zonally averaged SLP correlation with PC1 of NH SLP. Contour intervals: (a), (d) 1 hPa; (b), (e) 0.15. The zero contour is omitted.

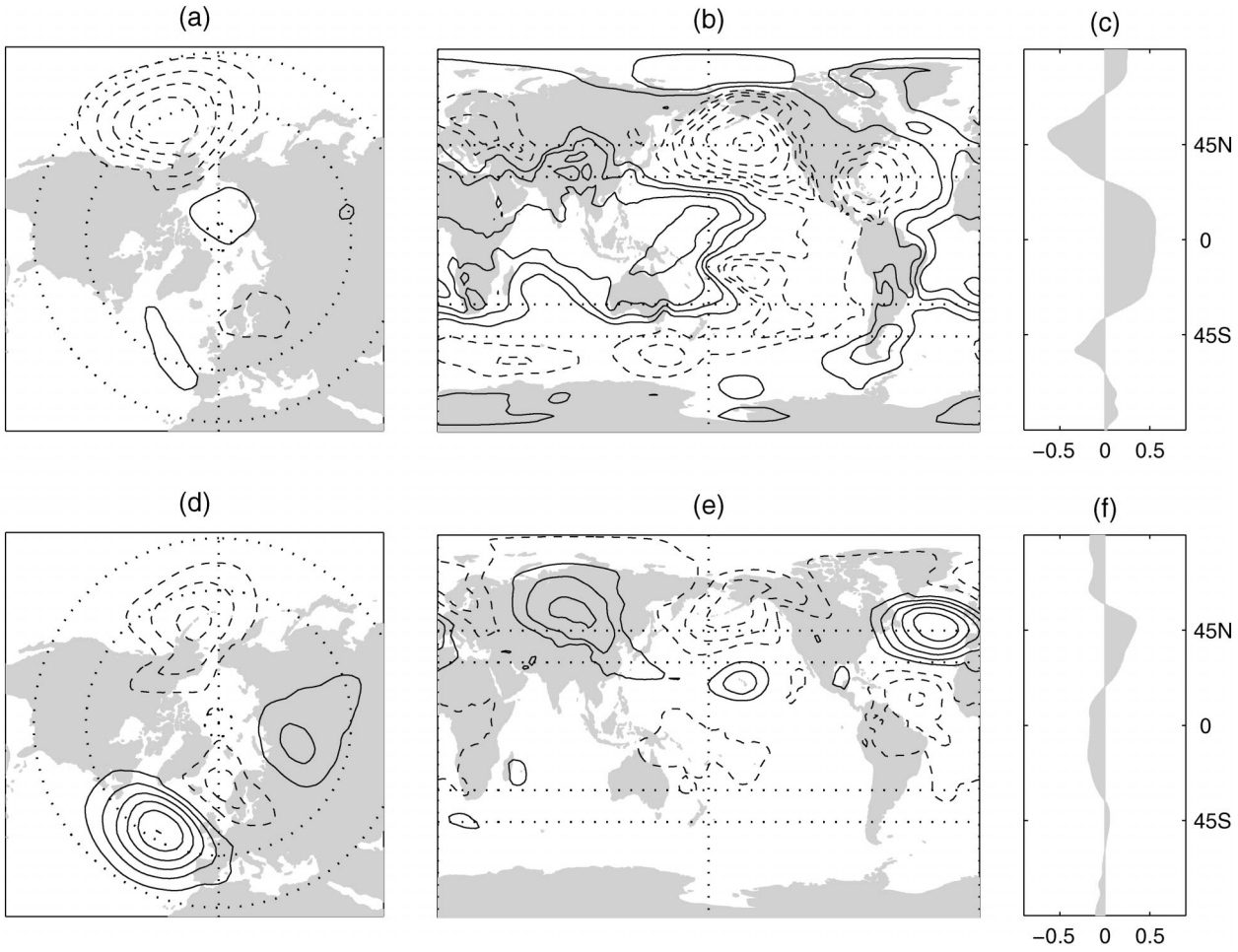

FIG. 14. As in Fig. 13 but for the NH SLP PC2.

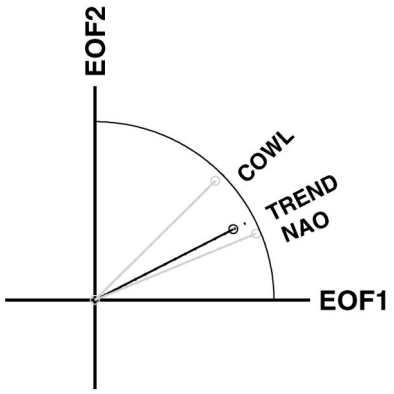

FIG. 15. As in Fig. 4a but for the spatial pattern of the observed SLP trend projected on the EOFs of the detrended monthly SLP field. For reference, projections of the NAO and COWL patterns are also shown in gray.

intraseasonal Northern Hemisphere variability are compared in Figs. 13a,d. The former is NAO-like, whereas the latter exhibits a strong Pacific center, as in the NAM. Pronounced differences are also evident in the correlation between PC1 and SLP over the remainder of the globe, as shown in Figs, 13b,c,e,f. Correlations with the Tropics and Southern Hemisphere are much stronger on interannual time scales, particularly in zonally averaged SLP. However, the correlations of EOF1 with the Tropics decrease significantly when the EOF analysis is performed on detrended winter-averaged SLP data.

Figure 14 shows corresponding patterns for EOF2. The pattern of the interannual variability is localized over the Pacific sector and it is clearly linked to the distinctive signature of the Southern Oscillation (e.g., Trenberth and Shea 1987), with a temporal correlation coefficient of -0.61 with the Southern Oscillation index. As is the case for EOF1, significant correlations extend into the Tropics, suggestive of global structure. The corresponding global regression pattern for 200-hPa streamfunction for interannual PC2 (not shown) exhibits distinctive equatorially symmetric anticyclonic

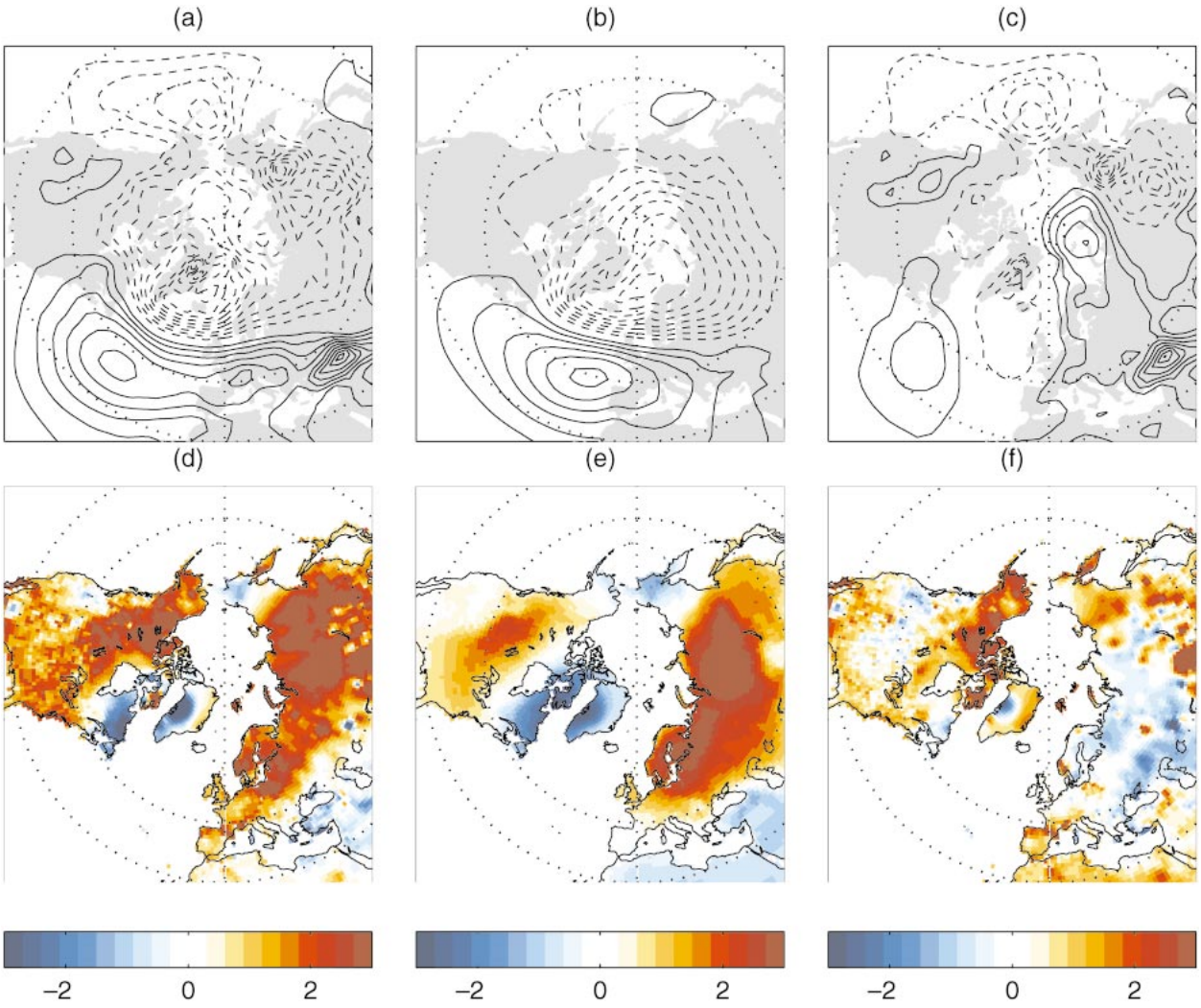

FIG. 16. (a)–(c) SLP and (d)–(f) SAT wintertime (DJFM) 1958–99 trends. (a), (d) Linear trend. (b), (e) The component of that trend that is linearly congruent with the two leading PCs of the detrended SLP field. (c), (f) The residual trend. SLP contour interval 1 hPa; the zero contour is omitted.

gyres over the Pacific sector, also reminiscent of the pattern associated with ENSO. In contrast, the intraseasonal pattern is suggestive of Rossby wave trains trapped in extratropical northern latitudes. The extratropical atmospheric SLP signature of the pattern that Mantua et al. (1997) refer to as the Pacific decadal oscillation, formed by regressing SLP onto the leading PC of Pacific sea surface temperature poleward of 20°N, is also localized in the Pacific sector, consistent with the signature of the interannual EOF2 (not shown).

TABLE 3. As in Table 2 but for 1925–99 SLP data.

	v/v_m	$(PC1 + PC2)_m$	PC1 + PC2
Monthly	1	34	34
Seasonal	0.38	43	44
5-yr mean	0.12	52	52

8. SLP and SAT trends

SLP trends over different periods and regions have been documented in several recent studies. Trenberth and Hurrell (1994) noted a decrease of the Aleutian low pressure in the decade from 1976 to 1988; Walsh et al. (1996) reported a decrease in SLP over the Arctic from 1979 to 1994, and Gillett et al. (2003) documented the global 1948–98 SLP trend. SAT trends have been documented in numerous studies, including Houghton et al. (2001).

This section documents the relation between the observed hemispheric SLP and SAT trends and the trends detected in the time series of the two SLP leading PCs. Averaged over the Northern Hemisphere, the mean-square amplitude of the observed SLP trend since 1958 (estimated by summing over all grid points, weighting by the cosine of latitude) is larger than any of the 1000

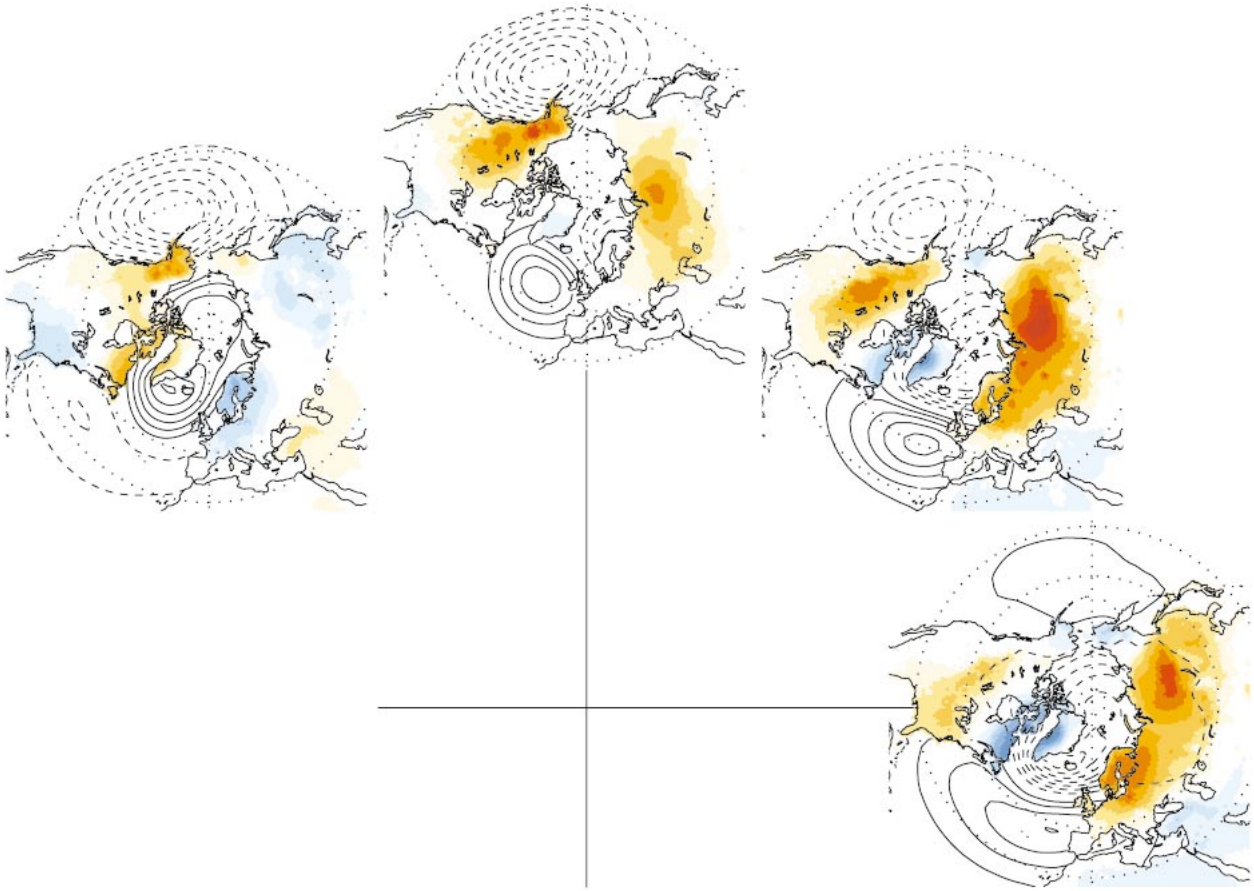

FIG. 17. SLP (contours) and SAT (shading) patterns associated with 1 std dev anomaly of the time series of the linear combinations of SLP PCs 1 and 2 corresponding to angles of 0°, 45°, 90°, and 135° with the SLP PC1 axis. SLP contour every 1 hPa, SAT shading every 0.4°C; warm colors indicate positive anomalies.

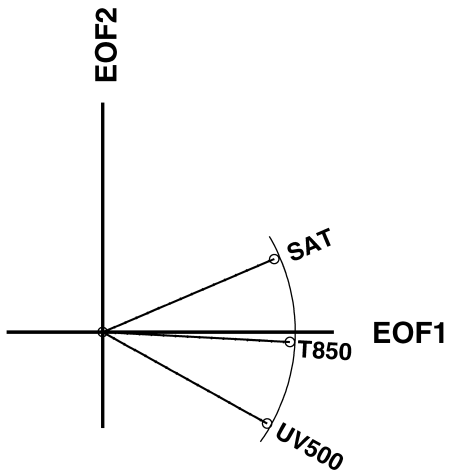

FIG. 18. Projections (area-weighted spatial correlations) of patterns associated with the leading EOF of SAT, T850, and the concatenated fields of 500-hPa u and v, with the phase space defined by the two leading EOFs of monthly DJFM NH SLP anomalies, north of 20°N.

synthetic trends generated by randomly scrambling the chronological order of the winters. Based on a conventional t test, the trends in PCs1 and 2 of SLP are significant at the 99% and 95% levels, respectively. The linear combination of PCs1 and 2 that exhibits the largest trend is significant at the 99.9% level.

To project the SLP trend pattern upon the two-dimensional phase space, the SLP data were linearly detrended before computing the EOFs in order to ensure that the phase space is not in any way influenced by the existence of the trend.[4] The result is shown in Fig. 15.

In agreement with previous studies of Hurrell (1995) and Thompson et al. (2000) the pattern of SLP trends projects strongly upon the NAO and upon PC1, the index of the NAM. The angle in this two-dimensional phase space coincides almost perfectly with that of the NAO.

The spatial patterns of the observed trends in SLP and SAT, their projection upon the least squares best-fit linear combination of the two leading PCs of the SLP

[4] The EOFs of detrended data are rotated clockwise by an angle of about 10° in the phase space of Fig. 4.

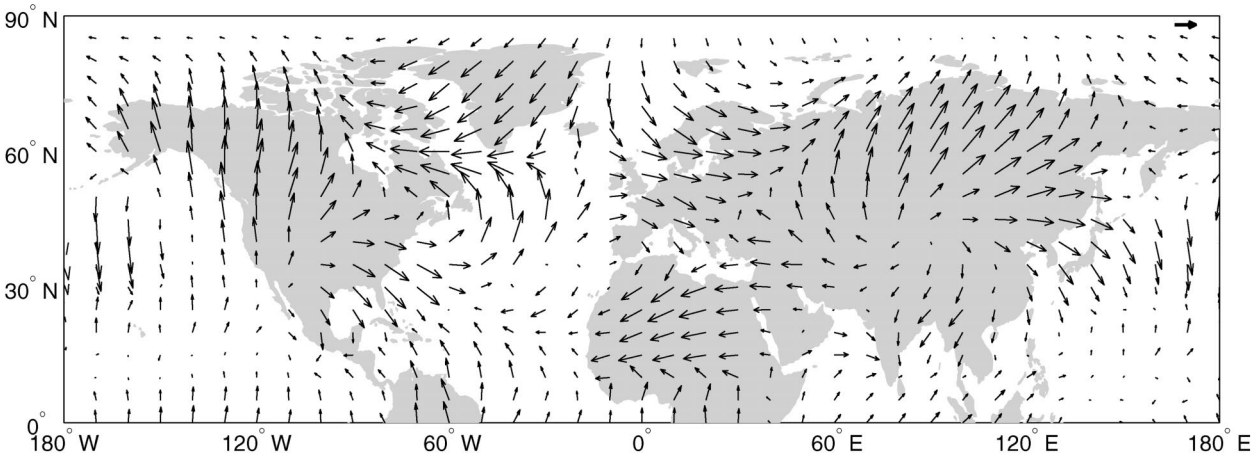

FIG. 19. Vectorial representation of correlations between monthly mean 850-hPa temperature and PCs 1 (*x* component) and 2 (*y* component) of monthly DJFM SLP anomalies. The vector in the upper-right corner represents a correlation coefficient of 0.5.

detrended dataset, and the residual trend are shown in Fig. 16. The resemblance between the spatial pattern of the SLP trend and its projection upon the PCs is quite striking. The residual trend does not exhibit a coherent, planetary-scale structure, and its hemispherically averaged mean-square amplitude is typical of those in trend patterns derived from the temporally scrambled data.

The bottom row of Fig. 16 show corresponding results for SAT. A very large fraction of the regional SAT trends can be accounted for on the basis of the trends in the SLP PCs, and the pattern of residual trend is patchy, with warming in some areas and cooling in others.

9. Discussion

The foregoing results serve to emphasize the strong contribution of the two leading PCs of the NH SLP field

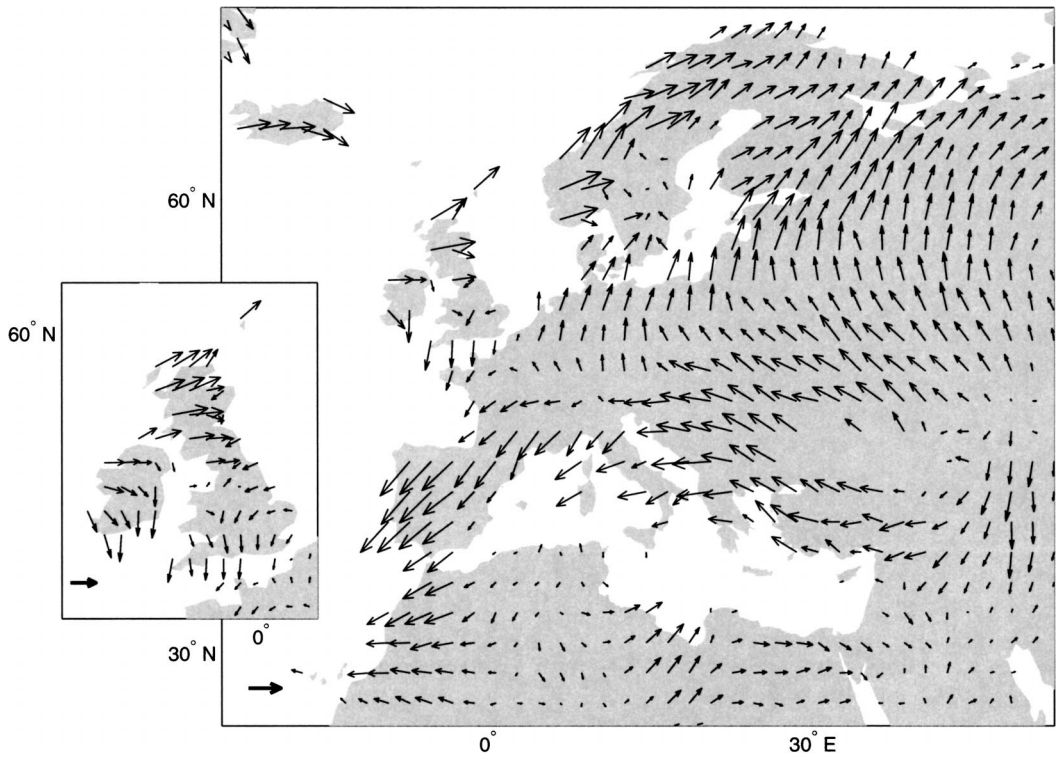

FIG. 20. Vectorial representation of correlations between monthly mean SLP and PCs 1 (*x* component) and 2 (*y* component) of monthly precipitation anomalies over Europe (2° × 2°) and British Isles at a higher resolution (1° × 1°). The vector in the lower-left corner corresponds to a correlation coefficient of 0.5.

to the wintertime low-frequency variability. Together, these patterns account for over one-third of the variance of the monthly mean SLP field, around half of the variance of the wintertime mean SLP field, over two-thirds of the variance of five-winter mean SLP field, and virtually all the coherent, planetary-scale structure in the 1958–99 winter SLP trend pattern. Analogous statistics based on the Trenberth's data for the period of record 1925–99 are shown in Table 3. The increasing prominence of these patterns as one progresses from intraseasonal to interannual to interdecadal time scales suggests that they play an important role in the wintertime SLP and SAT variability on time scales of centuries and longer. That the percentages of the variance explained by PCs1 and 2 for the 1958–99 data are higher than for the period 1925–99 may be a reflection of the fact that the strong NH SLP trends observed from the 1950s onward project strongly upon the leading EOFs of NH SLP.

Depending upon how these two patterns are juxtaposed at any given time, the associated SLP and SAT patterns can assume a variety of forms, as illustrated in Fig. 17. For example, phase angles near 45°/225° denote a strengthening or weakening of the Icelandic and Aleutian lows accompanied by anomalous warmth or coolness over both Eurasia and North America poleward of 40°N; angles near 135°/315° denote a seesaw between the intensities of the two lows accompanied by anomalous warmth of one continent and coolness of the other; angles near 0°, 90°, 180°, and 270° denote more regional patterns, with SLP anomalies focused on a single ocean and the associated SAT anomalies over the downstream continent. On the basis of linear combinations of these two patterns it is possible to reconstruct the SLP patterns associated with the NAO, PNA, and AIS teleconnection patterns, the COWL pattern. Although the structure of the two leading EOFs of the geopotential height field varies with height, these changes are principally due to rotation of the patterns within a common two-dimensional phase space; that is, the leading EOFs at different levels are linear combinations of the same two basic patterns. The two leading SLP PCs account for over 90% of the variance of the two leading geopotential height PCs at levels up to 500 hPa and over 80% at levels up to 200 hPa.

The SLP patterns associated with the leading PC of other fields than geopotential height can also be represented in the two-dimensional phase space. The spatial pattern derived by projecting the SLP field onto the time series of PC1 of lower-tropospheric temperature (850 hPa) is almost identical to the pattern of SLP EOF1. The SLP patterns corresponding to the leading PC of surface air temperature and to the concatenated (considered together) u and v components of the 500-hPa wind project almost perfectly onto the phase space as well. These relationships are documented in Fig. 18. The correlation coefficient between the time series of temperature and wind PC1 and their respective best-fit linear combination of SLP PCs1 and 2 are 0.82 and 0.89.

In combination, the two leading SLP PCs also account for substantial fractions of the variance of winter monthly mean surface air temperature and precipitation throughout most of the NH. Lower-tropospheric temperature (Fig. 19) is strongly correlated with PC1 over Europe, North Africa, parts of East Asia and the eastern United States and eastern Canada, and with PC2 over the high-latitude oceans and western North America. Precipitation (Fig. 20) exhibits a more complex pattern. For example, from the inset it is evident that over Scotland the high index of the NAO, which corresponds to an angle of $\sim 15°$ in the phase space, is conducive to heavy precipitation, but along the east coast of England the relationship is weak and in the opposite sense. Trigo et al. (2002) observed a similar relationship for cloud cover. In the south of England and Ireland the negative polarity of EOF2, which favors an anomalous southerly flow, is dominant. Some of this regional variability is attributable to the structure of the SLP EOFs, but part of it represents a response to more regional terrain features. For example, westerly wind anomalies, as observed in association with the high index polarity of the NAO, favor enhanced precipitation over England, with the notable exception of the low-lying eastern coastal region, where easterly rather than westerly wind anomalies favor above normal precipitation. The strong gradients across the Alps and Scandinavia in the larger figure are also indicative of terrain-induced fine structure that is more clearly revealed in regional maps (not shown).

There is no guarantee that the spatial patterns that emerge in EOF analysis correspond to dynamical modes of variability. Mindful of this distinction, we have referred to EOFs 1 and 2 of the SLP fields as patterns, rather than modes. Previous investigations offer some insights into the dynamical interpretation of these patterns. Results of Feldstein and Lee (1998), Limpasuvan and Hartmann (2000), and Lorenz and Hartmann (2003) suggest that the structure of EOF1 derives mainly from the interactions between the eddies and the zonal flow, whereas results of Simmons et al. (1983) suggest that the prominence of the second PNA-like EOF relative to other eddy patterns derives from the structure of the zonally varying climatological-mean flow at the jet stream level. The SLP EOFs for the SH are consistent with this interpretation. During the austral winter (June–August) EOF1, the southern annular mode (SAM; Gong and Wang 1999; Thompson and Wallace 2000) accounts for 30% of the variance on the month-to-month time scale, while EOF2, the Pacific–South America (PSA) pattern which is in some sense analogous to the NH PNA pattern, accounts for 13%. In contrast, during the austral summer (DJF), when the climatological-mean basic state is more zonally symmetric, EOF1 (the SAM) accounts for 35% of the variance and the fraction explained by EOF2 drops to 8%.

We have shown that the structure of leading EOFs of the interannual and intraseasonal variability of SLP are different in two respects: 1) the interannual EOFs tend to be localized over Atlantic and Pacific sectors, whereas the second intraseasonal EOF is suggestive of a coupling between the PNA wave train and another wave train emanating from the Atlantic sector and extending across Eurasia, and 2) the intraseasonal EOFs are largely trapped within the NH extratropics, whereas the interannual EOFs appear to be hemispheric expressions of global patterns, one of which is clearly ENSO related. Placing the hemispheric results in a global context is a challenge for future research.

10. Concluding remarks

The main message of this paper is that much of the structure inherent in the NH wintertime geopotential height, temperature, and precipitation fields on time scales of months and longer can be represented in terms of just two planetary-scale patterns. Our choice of SLP as opposed to, say, 500-hPa height for defining the phase space is motivated by the fact that the eigenvalues are more clearly separated, yielding a sharper, more reproducible definition of the coordinate axes.[5] It is also notable that EOF1 of SLP is virtually identical to the SLP pattern observed in association with the leading EOF of lower-tropospheric temperature and the geopotential height at the lower-stratospheric levels. Using PCs and EOFs as axes offers the additional advantage that the leading patterns are orthogonal to one another in both the time and space domains. Alternatively, the coordinate axes could be chosen to correspond with NAO and PNA patterns, as suggested by Ambaum et al. (2001). An objective way of defining this ''NAO/PNA'' phase space is to perform a varimax rotation of PCs1 and 2, which, by construction, yields the simplest possible linear combinations of the EOFs. The nonorthogonal axes obtained through a varimax rotation in this two-dimensional phase space are located about halfway between the EOF1/EOF2 and the NAO/PNA sets of axes (not shown). The phase space could be also defined on the basis of interannual EOFs, in which case, it would correspond more closely with the NAO and PNA patterns.

On the basis of rotated principal component analysis of the interannual variability of the 500-hPa height field Kushnir and Wallace (1989) concluded that only two modes stand out above the background continuum: the NAO and the PNA pattern. The consistency between the conclusions of our study and theirs, despite the differences in methodology, lends credence to the notion that true hemisphere ''teleconnection patterns'' are much more limited in number than the acronyms used to label them. Much of the redundancy is due to the time-honored reliance on subjectively defined ''primitive indices'' as a basis for naming and characterizing patterns of variability. When the corresponding spatial patterns and projection indices are considered, the linear dependence of many of these so-called modes becomes readily apparent. On the other hand, we would not go so far as to claim that EOFs of order higher than the second are dynamically unimportant. For example EOF3 of SLP is associated with an upper-level wave train extending from the tropical Atlantic to Indonesia all the way across Eurasia along a great circle route. EOFs 4 and 5 capture variability over the Pacific sector related to the ''North Pacific Oscillation'' of Walker and Bliss (1932) and the ''Western Pacific pattern'' of WG. Collectively, these three patterns account for ~25% of the month-to-month variance. They play important roles in the intraseasonal variability but their contribution to the total variance on longer time scales is substantially smaller.

The methodology described in this paper is well suited for assessing and comparing the performance of climate models with regard to their ability to simulate the naturally occuring patterns of climate variability.

That the leading EOFs of the SLP field become increasingly prominent as the averaging interval increases from a month to a season, and from a single winter season to five winter seasons suggests that the leading EOFs might be even more prominent in means of ensemble simulations of twentieth-century climate variability such as those performed for the Atmospheric and Coupled Model Intercomparison Projects (AMIP, CMIP). Furthermore, one might expect the prominence of these modes to increase with the size of the ensemble, or in experiments simulating anthropogenic climate change. It will be interesting to see if this is the case.

Acknowledgments. This work was supported by the National Science Foundation under Grant ATM 0318675. We would like to thank Dr. Kevin Trenberth and an anonymous reviewer for their incisive, thorough, and insightful comments.

[5] In the Monte Carlo test described at the end of section 3, for our sample size of 168 months, the rms error in the definition of the axes is 17° for the 500-hPa EOFs, compared to 7° for the SLP EOFs. This result is consistent with the algebraic derivation of the sampling error in eigenvectors given in Quadrelli et al. (2004, manuscript submitted to *J. Climate*).

REFERENCES

Ambaum, M. H. P., B. J. Hoskins, and D. B. Stephenson, 2001: Arctic Oscillation or North Atlantic Oscillation? *J. Climate,* **14,** 3495–3507.

Barnston, A. G., and R. E. Livezey, 1987: Classification, seasonality, and persistence of the low-frequency atmospheric circulation patterns. *Mon. Wea. Rev.,* **115,** 1083–1126.

Cheng, X., and J. M. Wallace, 1993: Cluster analysis of the Northern Hemisphere wintertime 500-hPa height field: Spatial patterns. *J. Atmos. Sci.,* **50,** 2674–2696.

——, G. Nitsche, and J. M. Wallace, 1995: Robustness of low-frequency circulation patterns derived from EOF and rotated EOF analyses. *J. Climate,* **8,** 1709–1720.

Feldstein, S. B., and S. Lee, 1998: Is the atmospheric zonal index driven by an eddy feedback? *J. Atmos. Sci.,* **55,** 3077–3086.
Gillett, N. P., F. W. Zwiers, A. J. Weaver, and P. A. Stott, 2003: Detection of human influence on sea level pressure. *Nature,* **422,** 292–294.
Gong, D., and S. Wang, 1999: Definition of Antarctic Oscillation index. *Geophys. Res. Lett.,* **26,** 459–462.
Honda, M., and H. Nakamura, 2001: Interannual seesaw between the Aleutian and Icelandic lows. Part II: Its significance in the interannual variability over the wintertime Northern Hemisphere. *J. Climate,* **14,** 4512–4529.
——, ——, J. Ukita, I. Kousaka, and K. Takeuchi, 2001: Interannual seesaw between the Aleutian and Icelandic lows. Part I: Seasonal dependence and life cycle. *J. Climate,* **14,** 1029–1042.
Houghton, J. T., Y. Ding, D. J. Griggs, M. Noguer, P. J. van der Linden, X. Dai, K. Maskell, and C. A. Johnson, Eds., 2001: *Climate Change 2001: The Scientific Basis.* Cambridge University Press, 892 pp.
Hurrell, J. W., 1995: Decadal trends in the North Atlantic Oscillation: Regional temperatures and precipitation. *Science,* **269,** 676–679.
Kalnay, E., and Coauthors, 1996: The NCEP/NCAR 40-Year Reanalysis Project. *Bull. Amer. Meteor. Soc.,* **77,** 437–471.
Kidson, J. W., 1975: Eigenvector analysis of monthly mean surface data. *Mon. Wea. Rev.,* **103,** 177–186.
Kushnir, Y., and J. M. Wallace, 1989: Low-frequency variability in the Northern Hemisphere winter: Geographical distribution, structure and time-scale dependence. *J. Atmos. Sci.,* **46,** 3122–3142.
Kutzbach, J., 1970: Large-scale features of monthly mean Northern Hemisphere anomaly maps of sea-level pressure. *Mon. Wea. Rev.,* **98,** 708–716.
Limpasuvan, V., and D. L. Hartmann, 2000: Wave-maintained annular modes of climate variability. *J. Climate,* **13,** 4414–4429.
Lorenz, D. J., and D. L. Hartmann, 2003: Eddy-zonal flow feedback in the Northern Hemisphere winter. *J. Climate,* **16,** 1212–1227.
Mantua, N., S. Hare, Y. Zhang, J. Wallace, and R. C. Francis, 1997: A Pacific interdecadal climate oscillation with impacts on salmon production. *Bull. Amer. Meteor. Soc.,* **78,** 1069–1079.
Molteni, F., A. Sutera, and N. Tronci, 1988: The EOFs of the geopotential eddies at 500 mb in winter and their probability density distributions. *J. Atmos. Sci.,* **45,** 3063–3080.
North, G. R., T. L. Bell, R. F. Cahalan, and F. J. Moeng, 1982: Sampling errors in the estimation of empirical orthogonal functions. *Mon. Wea. Rev.,* **110,** 699–706.
Rogers, J., and M. McHugh, 2002: On the separability of the North Atlantic Oscillation and Arctic Oscillation. *Climate Dyn.,* **19,** 599–608.
Simmons, A. J., J. M. Wallace, and G. Branstator, 1983: Barotropic wave propagation and instability, and atmospheric teleconnection patterns. *J. Atmos. Sci.,* **40,** 1363–1392.
Thompson, D. W. J., and J. M. Wallace, 1998: The Arctic Oscillation signature in the wintertime geopotential height and temperature fields. *Geophys. Res. Lett.,* **25,** 1297–1300.
——, and ——, 2000: Annular modes in the extratropical circulation. Part I: Month-to-month variability. *J. Climate,* **13,** 1000–1016.
——, ——, and G. C. Hegerl, 2000: Annular modes in the extratropical circulation. Part II: Trends. *J. Climate,* **13,** 1000–1016.
Trenberth, K. E., 1984: Signal versus noise in the Southern Oscillation. *Mon. Wea. Rev.,* **112,** 326–332.
——, and D. Paolino Jr., 1980: The Northern Hemisphere sea-level pressure data set: Trends, errors and discontinuities. *Mon. Wea. Rev.,* **108,** 855–872.
——, and ——, 1981: Characteristic patterns of variability of sea level pressure in the Northern Hemisphere. *Mon. Wea. Rev.,* **109,** 1169–1189.
——, and D. J. Shea, 1987: On the evolution of the Southern Oscillation. *Mon. Wea. Rev.,* **115,** 3078–3096.
——, and J. Hurrell, 1994: Decadal atmosphere–ocean variations in the Pacific. *Climate Dyn.,* **9,** 303–319.
Trigo, R. M., T. J. Osborn, and J. M. Corte-Real, 2002: The North Atlantic Oscillation influence on Europe: Climate impacts and associated physical mechanisms. *Climate Res.,* **20,** 9–17.
Walker, G. T., and E. W. Bliss, 1932: World weather. *Mem. Roy. Meteor. Soc.,* **4,** 53–84.
Wallace, J. M., and D. S. Gutzler, 1981: Teleconnections in the geopotential height field during the Northern Hemisphere winter. *Mon. Wea. Rev.,* **109,** 784–812.
——, and D. W. J. Thompson, 2002: The Pacific center of action of the Northern Hemisphere annular mode: Real or artifact? *J. Climate,* **15,** 1987–1991.
——, Y. Zhang, and J. Renwick, 1995: Dynamic contribution to hemispheric mean temperature trends. *Science,* **270,** 780–783.
Walsh, J. E., W. L. Chapman, and T. L. Shy, 1996: Recent decrease of sea level pressure in the central Arctic. *J. Climate,* **9,** 480–486.
Wang, J., and M. Ikeda, 2000: Arctic Oscillation and Arctic Sea-Ice Oscillation. *Geophys. Res. Lett.,* **27,** 1287–1290.
Willmott, C. J., and S. M. Robeson, 1995: Climatologically Aided Interpolation (CAI) of terrestrial air temperature. *Int. J. Climatol.,* **15,** 221–229.